19th International Conference on
Harmonisation within Atmospheric Dispersion Modelling for Regulatory Purposes
3-6 June 2019, Bruges, Belgium

TURBULENT SCHMIDT NUMBER ESTIMATE OVER URBAN CANOPIES

Annalisa Di Bernardino[1], Paolo Monti[1], Giovanni Leuzzi[1], Fabio Sammartino[1] and Giorgio Querzoli[2]

[1]Dipartimento di Ingegneria Civile Edile e Ambientale, Università di Roma "La Sapienza", Roma, Italy
[2]Dipartimento di Ingegneria del Territorio, Università di Cagliari, Cagliari, Italy.

Abstract: This work presents laboratory estimates of the turbulent Schmidt number (Sc_t) above an idealized three-dimensional urban canopy. To do this, a neutral atmospheric boundary layer has been reproduced in the water channel and a staggered array of cubic obstacles of equal heights placed on the channel bottom has been used to simulate the canopy. A point source emitted a passive tracer at a constant rate above the cube array. Simultaneous measurements of pollutant concentration and velocity permitted the estimation of the vertical fluxes of mass and momentum and, therefore, of Sc_t. The results show a clear dependence of Sc_t on the height above the canopy.

Key words: *Water channel; PLIF; Concentration fluctuations; Pollutant dispersion; Urban canopy.*

INTRODUCTION

Urban environments are usually studied (numerically and experimentally) by considering simplified building geometries by using arrays of obstacles with archetypal arrangements (Oke, 1988; Badas et al., 2018). Since pollutant dispersion in cities is mostly investigated numerically through Reynolds-Averaged Navier-Stokes models, a question arises regarding the values to assign to the turbulent mass and momentum fluxes in the governing equations. These unknowns are currently modelled by using first-order closures, which involve the definition of exchange coefficients such as the eddy diffusivities of momentum (K_M) and mass (D_t). In current practice, K_M is assumed proportional to the turbulent kinetic energy and to its rate of dissipation, while $D_t = K_M(Sc_t)^{-1}$, where Sc_t is the turbulent Schmidt number. The choice of Sc_t is not straightforward and influences considerably the numerical results. It must be set prior the simulation and it is generally assumed to fall in the range 0.2-1.3 (Blocken et al., 2008). Experimental estimates of Sc_t require the simultaneous knowledge of turbulent fluxes of momentum and scalars, generally obtained in the laboratory (Monti et al., 2007; Carpentieri et al., 2012; Nosek et al., 2016; Tomas et al., 2017; Di Bernardino et al., 2018).

This study provides information on Sc_t above a cube array with plan area index, λ_P=0.25. K_M and D_t were estimated from simultaneous measurements of velocity and pollutant concentration fields conducted in the water channel.

EXPERIMENTAL SETUP

Since acquisition techniques and data processing have been presented elsewhere (Di Bernardino et al. 2015, 2017), only the salient features are briefly reviewed here. A neutral boundary layer is recreated in a water channel 7.4 m long having a rectangular cross section 0.35 m high and 0.25 m wide. The water depth and the free-stream velocity are 0.16 m and U=0.34 ms^{-1}, respectively. The roughness Reynolds number of the flow, $Re_\tau = u_{*,ref}H/\nu$, is about 250, where H=0.015 m is the cube height, $\nu=10^{-6}$ m^2s^{-1} is the kinematic viscosity of water and $u_{*,ref}$=0.017 ms^{-1} is the reference friction velocity, equal to the average of $\sqrt{-\overline{u'w'}}$ calculated over the constant flux layer (CFL, see Fig. 4). Here, u and w are the streamwise and the vertical velocity component, respectively, while the prime indicates the fluctuation and the bar the time average.

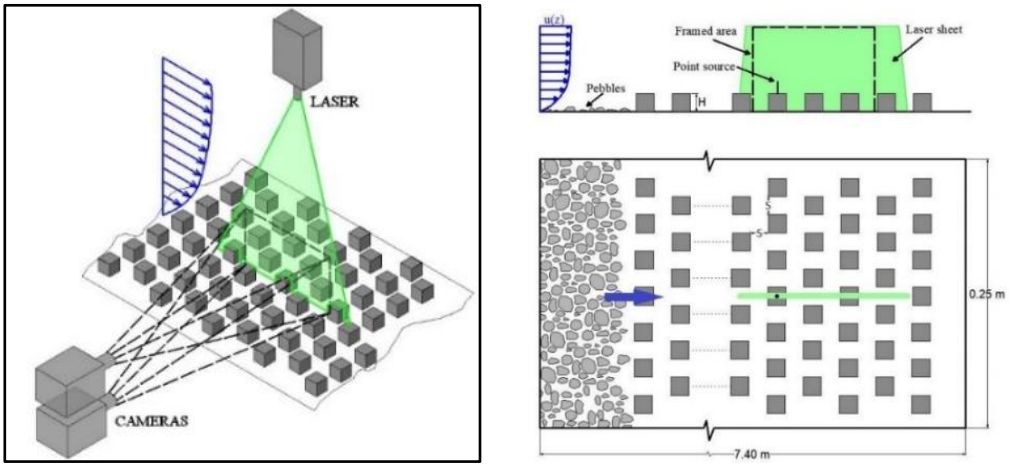

Figure 1. Layout of the experimental setup. The green line in the right panel is the signature along the horizontal plane of the vertical interrogation area.

The cube array is made of uniform, sharp-edged cubes glued onto the channel bottom in staggered pattern (Fig. 1). The test section is located about 5 m downstream of the inlet, where the boundary layer is fully developed. The plan area index of the array (λ_P =0.25) corresponds to the wake interference regime (Grimmond and Oke, 1999), which is one of the most common geometries found in real cities (e.g. Salvati et al., 2019, Ferrari et al. 2017). The tracer was emitted continuously from a pipe inserted through a hole in the centre of the upwind building belonging to the interrogation area. The point source was located at a height (z) of 1.67H, was round (diameter 1 mm) and emitted a mixture of Rhodamine-WT and water delivered to the source by gravity (concentration at the source: $c_0=2.5\cdot10^{-3}$ kg m^{-3}; source mass rate $Q=11.9x10^{-11}$ kg s^{-1}). The streamwise and vertical velocity components and the tracer concentration (c) are measured simultaneously on the vertical section passing through the longitudinal axis of the channel (that is, the one passing through the source).

The acquisition facility consists of a laser (5 W, 532 nm) emitting a light sheet 2 mm thick illuminating the acquisition plane and two synchronized cameras (1024x1280 pixels, 250 Hz). The framed area is 102 mm wide (x-axis) and 82 mm high (z-axis). The first camera acquires the positions of the non-buoyant particles (20 μm in diameter) immersed in the fluid and allows the evaluation of the instantaneous velocity fields by means of a feature-tracking algorithm based on image analysis (Cenedese et al., 2005). A Gaussian interpolation algorithm (Cenedese et al., 2000) is applied for each time instant to the scattered samples on the x-z plane to obtain the instantaneous velocity field on a regular 205x164 array, which corresponds to a 0.5 mm spatial resolution (i.e. H/30). To sense only the fluorescent light emission, the second camera is equipped with a narrow band pass filter tuned on 587 nm (Rhodamine-WT is excited at 532 nm and emits at 587 nm).

Concentration values are achieved via planar laser-induced fluorescence (PLIF). The instantaneous concentration field is mapped onto the velocity field using an affine transformation to permit the investigation of the scalar flux. In this process, the superimposition of the velocity and concentration fields

is obtained by assigning to each grid cell the value of the concentration at the centre of the cell. 25,000 instantaneous velocity and concentration fields have been measured during the experiments, corresponding to a 100 s long acquisition. The mean, $\bar{c}$, of the Rhodamine-WT concentration is determined on each of the image pixels by means of Reynolds averaging. Similarly, the mean velocity components, $\bar{u}$ and $\bar{w}$, and the vertical momentum flux, $\overline{u'w'}$, were calculated in each node of the 205x164 array. On the latter grid, the turbulent vertical flux of the tracer, $\overline{w'c'}$, is determined.

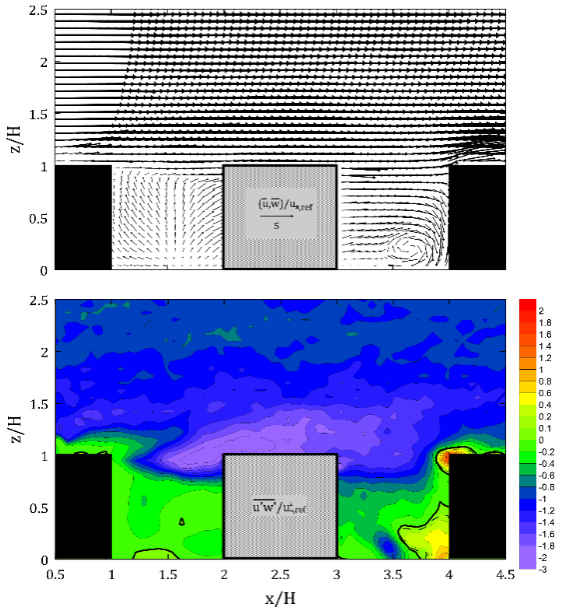

Figure 2. Normalized mean velocity (upper panel) and vertical momentum flux (lower) in the vertical plane passing through the middle of the cubes. The region of optical occlusion due to out-of-plane cubes is shown in grey.

RESULTS AND DISCUSSION

The vector field of the mean velocity in the vertical plane passing through the middle of the cubes is shown in the upper panel of Fig. 2. The values of the two components are normalized by $u_{*,ref}$. The mean flow resembles that already reported in other studies (e.g. Coceal et al., 2006), i.e. a current above the canopy nearly parallel to the streamwise direction, a recirculation in front of the windward wall of the obstacle in the bottom right-hand corner within the canyon and the absence of a recirculation behind the upwind obstacle. The normalized vertical momentum flux, $\overline{u'w'}/u^2_{*,ref}$, is negative everywhere except near the top edge of the downwind cube.

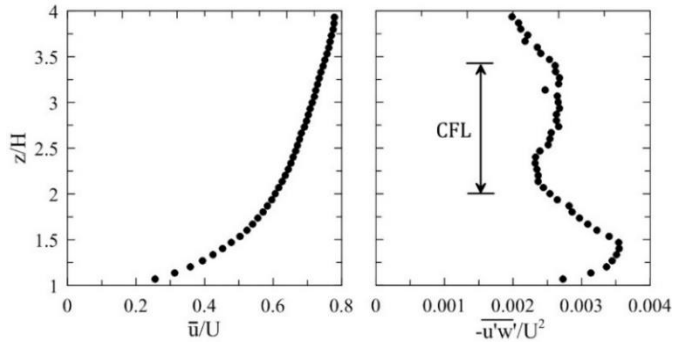

Figure 3. Vertical profiles of the normalized streamwise mean velocity (left panel) and vertical momentum flux (right) in the vertical plane passing through the middle of the cubes.

Figure 3 reports the vertical profiles of the normalized streamwise velocity component (left) and vertical momentum flux (right panel). These profiles were estimated by adopting the canopy approach (e.g.

Finnigan, 2000, Badas et al., 2017, Garau et al., 2018), i.e. by horizontally averaging the time averaged statistics over a region including one building top and the contiguous canyon. In doing so, the results can be assumed as representative of the repeating unit constituting the canopy. A constant flux layer forms in the range $1.8 \lesssim z/H \lesssim 3.5$, to which it is associated a friction velocity $u_{*,ref} = 0.017\ ms^{-1}$. The vertical profiles of the normalized turbulent vertical tracer flux, $\overline{w'c'}/u_{*,ref}c_*$, and mean concentration, $\bar{c}/c_*$, measured at two downstream positions are depicted in Fig. 4. Here, $c_* = Q/(H^2 u_{*,ref})$ is the reference concentration. It is apparent the correspondence of the location of the maximum $\bar{c}$ with the change in sign of $\overline{w'c'}$. This suggests that along the vertical the turbulent flux is always down gradient and, therefore, positive values of the eddy diffusivity of mass are everywhere associated to $\overline{w'c'}$, in analogy with molecular behaviour.

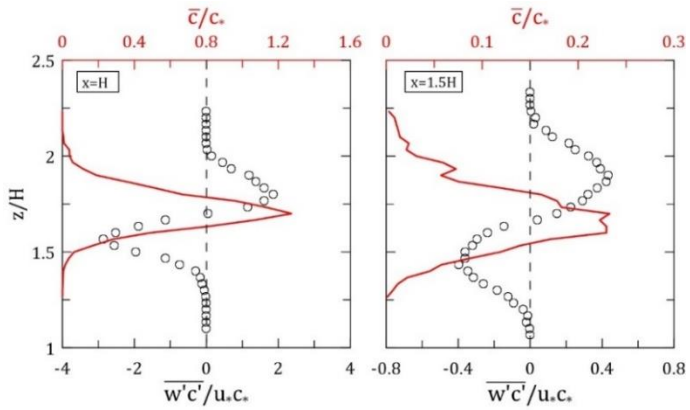

Figure 4. Vertical profiles of the normalized concentration ($\bar{c}/c_*$, red line) and vertical turbulent mass flux ($\overline{w'c'}/u_*c_*$, circles) taken at two downwind distances from the tracer source.

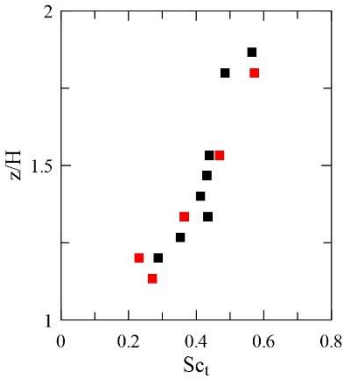

Figure 5. Vertical profiles of the turbulent Schmidt number at x=1.5H (black square) and x=2.5H (red square).

The mean concentrations and vertical fluxes described above can been used to estimate the eddy diffusivities of momentum and mass based on the gradient transport theory (or K-theory), viz.: $K_M = -\overline{u'w'}/(\partial\bar{u}/\partial z)$ and $D_t = -\overline{w'c'}/(\partial\bar{c}/\partial z)$ and, therefore, the turbulent Schmidt number:

$$Sc_t = K_M/D_t \tag{1}$$

It is important to underline that in current practice Sc_t is assumed as a constant set prior to numerical simulation. It is sometimes determined after a series of tests conducted at different Sc_t against experimental data (Blocken et al., 2008). The vertical profiles of Sc_t obtained in our experiments are shown in Fig. 5. In particular, Sc_t was calculated considering $\overline{w'c'}$ and $\bar{c}$ measured at x=1.5H (black squares) and x=2.5H (red), i.e. at two distances from the source long enough to assume that the size of the polluted plume is larger than the vortical structures characterizing the flow (see Harman and Finnigan (2008) for a discussion on the validity of K-theory for Sc_t estimates). To reduce errors due to oscillations of $\bar{c}$ along the vertical that can

have effects on $\partial\bar{c}/\partial z$ estimations, we smoothed the $\bar{c}$ profiles using a moving average interpolation. Furthermore, unrealistic D_t calculated in the region of the $\bar{c}$ maximum caused by $\partial\bar{c}/\partial z \approx 0$ have also been removed. Both the estimated Sc_t show a clear increase with height up to $z \approx 1.75H$, i.e. within the roughness sublayer, and share nearly the same profile. This supports the hypothesis that the two profiles have been taken in a region where Sc_t no longer depends on the downstream distance. The values obtained fall in the range 0.2-0.6, i.e. in line with other results reported in the literature in the case of flat terrain (Koeltzsch, 2000). Further investigation is needed to assess reliable Sc_t, taking also into consideration other array geometries.

REFERENCES

Badas, M.G., S. Ferrari, M. Garau, and G. Querzoli, G., 2017: On the effect of gable roof on natural ventilation in two-dimensional urban canyons. *J. of Wind Eng. Ind. Aerod.*, **162**, 24–34.

Badas, M.G., M. Garau, A. Seoni, S. Ferrari and G. Querzoli, 2018: Impact of rooftop stack configuration on 2D street canyon air quality. *J. Phys.*: Conf. Ser. 1110, 012003.

Blocken, B., T. Stathopoulos, P. Saathoff and X. Wang, 2008: Numerical evaluation of pollutant dispersion in the built environment: Comparison between models and experiments. *J. Wind Eng. Ind. Aerod*., **96**, 1817-1831.

Carpentieri, M., P. Hayden and A. G. Robins, 2012: Wind tunnel measurements of pollutant turbulent fluxes in urban intersections. *Atmos. Environ*., **46**, 669–674.

Cenedese, A., Z. Del Prete, M. Miozzi and G. Querzoli, 2005: A laboratory investigation of the flow in the left ventricle of a human heart with prosthetic, tilting-disk valves. *Exp. Fluids*, **39**, 322–335.

Cenedese, A., M. Miozzi and P. Monti, 2000: A laboratory investigation of land and sea breeze regimes. *Exp. Fluids*, **29**, S291–S299. DOI: 10.1007/s003480070031.

Coceal, O., T. G. Thomas, I. P. Castro and S. E. Belcher, 2006: Mean flow and turbulence statistics over groups of urban-like cubical obstacles. *Boundary-Layer Meteorol.*, **121**, 491-519.

Di Bernardino, A., P. Monti, P., G. Leuzzi and G. Querzoli, 2015: Water-channel study of flow and turbulence past a 2D array of obstacles. *Boundary-Layer Meteorol*., **155**, 73-85.

Di Bernardino, A., P. Monti, P., G. Leuzzi and G. Querzoli, 2017: Water-channel estimation of Eulerian and Lagrangian time scale of the turbulence in idealized two-dimensional urban canopies. *Boundary-Layer Meteorol*., **165**, 251-276.

Di Bernardino, A., P. Monti, G. Leuzzi and G. Querzoli, 2018: Pollutant fluxes in two-dimensional street canyons. *Urban Clim.*, **24**, 80-93.

Ferrari, S., M.G. Badas, M. Garau, A. Seoni and G. Querzoli, 2017: The air quality in narrow two-dimensional urban canyons with pitched and flat roof buildings. *Int. J. Environ. Pollut.*, **62**, 347-368.

Finnigan, J., 2000: Turbulence in plant canopies. *Annu. Rev. Fluid Mech*., **32**, 519–571.

Garau, M., Badas, M.G., Ferrari, S., Seoni, A., Querzoli, G., 2018: Turbulence and Air Exchange in a Two-Dimensional Urban Street Canyon Between Gable Roof Buildings. *Boundary-Layer Meteorol.* **167**, 123–143.

Grimmond, C. S. B. and T. R. Oke, 1999: Aerodynamic Properties of Urban Areas Derived from Analysis of Surface Form. *J. Appl. Meteorol*., **38**, 1261-1292.

Harman, I. N. and J. Finnigan. 2008: Scalar concentration profiles in the canopy and roughness sublayer. *Boundary-Layer Meteorol*., **129**, 323-351.

Koeltzsch, K., 2000: The height dependence of the turbulent Schmidt number within the boundary layer. *Atmos. Environ*., **34**, 1147-1151.

Monti, P., G. Querzoli, A. Cenedese and S. Piccinini, 2007: Mixing properties of a stably stratified parallel shear layer. *Phys. Fluids*, **19**, Article number 085104 (1-9). DOI: 10.1063/1.2756580.

Nosek, S., L. Kukačka, R. Kellnerová, K. Jurčàkovà and Z. Jaňour, 2016: Ventilation processes in a three-dimensional street canyon. *Boundary-Layer Meteorol.*, **159**, 259-284.

Oke, T., 1988. Street design and urban canopy layer climate. *Energy Build.*, **11**, 103-113.

Tomas, J. M., H. E. Eisma, M. J. B. M.·Pourquie, G. E. Elsinga, H. J. J. Jonker and J. Westerweel, 2017: Pollutant Dispersion in Boundary Layers Exposed to Rural-to-Urban Transitions: Varying the Spanwise Length Scale of the Roughness. *Boundary-Layer Meteorol.*, **163**, 225–251.

Salvati, A., P. Monti, H. Coch Roura and C. Cecere, 2019: Climatic performance of urban textures: analysis tools for a Mediterranean urban context. *Ener. Build.*, **185**, 162–179.